Desalination and Water Treatment
www.deswater.com
doi: 10.5004/dwt.2023.29781

302 (2023) 15–27
August

Effect of inlet temperature difference on water production and energy of direct contact membrane distillation for brackish water desalination

Abdullah Najib[a], Emad Ali[b,*], Jamel Orfi[a], Fahad Awjah Almehmadi[c]

[a]*Mechanical Engineering Department, King Saud University, P.O. Box: 800, Riyadh 11421, Saudi Arabia, emails: anmohammed@ksu.edu.sa (A. Najib), orfij@ksu.edu.sa (J. Orfi)*
[b]*Chemical Engineering Department, King Saud University, P.O. Box: 800, Riyadh 11421, Saudi Arabia, email: amkamal@ksu.edu.sa*
[c]*Department of Applied Mechanical Engineering, College of Applied Engineering, Muzahimiyah Branch, King Saud University, P.O. Box: 800, Riyadh 11421, Saudi Arabia, email: falmehmadi@ksu.edu.sa*

Received 30 March 2023; Accepted 8 July 2023

ABSTRACT

Membrane distillation is an emerging process that attracts real and increasing interest from academia and industry. It is powered by low grade thermal energy coming for example from waste heat or thermal renewable energy source. This work focuses on experimentally investigating the effect of the inlet temperature difference on the process performance. A membrane distillation unit is operated under coordinated variable inlet temperatures at a fixed difference. Specifically, fixed differences between the inlet feed and permeate temperature of 30°C, 40°C, and 50°C were experimentally examined. It is found that a wider inlet temperature difference promotes higher mass flux because it implicitly widens the driving force. 30% enhancement in the mass flux can be obtained by increasing the temperature difference from 30°C to 50°C. Despite being operated under a fixed temperature difference, raising the top brine temperature improves water production because vapor pressure increases exponentially with temperature. The mass flux can be increased by 25% and 125% when the inlet temperature differences increased from 30°C to 40°C and 50°C, respectively. Raising the top brine temperature also reduces both heating and cooling energy consumption as well as increases energy efficiency. It is also found that a top brine temperature of 80°C and an inlet cold temperature of 30°C is more beneficial than using an inlet permeate temperature of 15°C in the sense of 40% lower specific heating consumption, 15% less specific cooling consumption, and 21% higher thermal energy efficiency.

Keywords: Membrane distillation; Water desalination; Feed distribution; Productivity; Multistage

1. Introduction

Bodell was the first to introduce membrane distillation (MD) for the conversion of the brackish solution into drinkable water [1]. Since then MD became one of the most rapidly developing techniques in the separation industry [2]. MD combines thermal and membrane separation methods to withdraw water vapor from saline solutions using a hydrophobic microporous membrane. The vapor pressure difference across the membrane is the main driving force for water vapor transport through the membrane pores. The vapor pressure difference is directly proportional to the temperature difference between the cold and hot sides. MD gained wide recognition because it possesses several attractive characteristics; for example, it operates at modest operating conditions such as a low temperature of (30°C~80°C)

* Corresponding author.

[2] and atmospheric pressure [3,4]. This feature enabled MD to be powered by waste/low-grade energy sources [2,5,6]. MD can reject 100% of dissolved non-volatile ions and is resilient to concentrated feed solution [7]. It is reported that increasing the salinity from 0.5% to 10% would result in a minor reduction in water vapor flux [8]. Compared to reverse osmosis, MD is considered more applicable for treating high-salinity water [3,9]. It is reported that MD was used to handle very concentrated liquids generated from oil and gas removal, landfill sedimentary and reverse osmosis reject brine [6]. Besides, MD is used to alleviate industrial reject brine to attain zero liquid discharge [10,11]. Additional MD advantages include lower capital cost [12], comparatively less fouling opportunity and less pumping power consumption than reverse osmosis [6], simplicity, little external energy demands [13], and can survive full dry out and easily scalable [14]. Direct contact membrane distillation (DCMD) is one of the MD variations which is characterized by having the hot and cold streams in direct contact at the membrane interface. DCMD can be easily configured in a multistage structure, demands less energy, and generates a high-water mass flux [13,15,16]. DCMD has additional features such as application simplicity [17] and attaining a high gain output ratio if carefully tuned [14]. Generally, MD is bogged down in a wide spectrum of industrial implementation [18–27].

Although MD possesses appealing properties and versatile applications, it is still subject to downsides. For example, MD may exhibit membrane pore wetting [28], low single-pass recovery ratio (5%~10%) [14,29–31], flux degradation because of fouling [32,33], in addition to significant specific energy consumption [34] which can reach 39–69 kWh/m^3 [35] compared to reverse osmosis which has a much lower specific energy consumption reaching 2.5–5 kWh/m^3. These shortcomings and the rivalry with other competitive desalination technologies hindered the wide commencement of MD especially in the desalination industry [2]. Yet, the partial industrial commercialization of MD began evolving. GE and Memsys Cleanwater Pvt., Ltd. (Germany), commenced a pilot plant of 50 m^3/d capacity to treat wastewater with a salinity range between 150 to 230 g/L [36]. Another compact MD plant is deployed in the Maldives to process 10 m^3/d of produced water [30].

The minor industrial commencement of MD and its technical weaknesses triggered ample research activities in academia and industry to overcome these issues. For instance, numerous researchers investigated MD development to cure specific deficits and/or improve its performance to surpass the modern desalination methods in terms of reliability and economic efficiency. In fact, some studies targeted membrane fabrication such that can endure fouling, increase vapor transport, elongate the membrane life, etc. [37–39]. Others focused on an in-depth understanding of the implied heat and mass transfer mechanism [13,40,41], enhancing energy effectiveness by retrofitting and/or proposing novel configurations [42,43], implementing heart recovery systems [44,45], or brine recycling [46]. Some researchers have investigated the reduction of energy consumption costs by incorporating renewable energy such as solar energy [47–49] and low-grade heat [50,51]. On another hand, some investigators relied on adjusting the hydrodynamics conditions by manipulating the flow velocity to stimulate higher vapor flux [52] or as a means for scale/fouling prevention [53,54]. On another level, hybridizing MD with other desalination technologies either in an integrated framework or in sequential steps is also considered to increase the overall productivity and/or recovery ratio [55–57].

The concept of multistage or multiple effects which are typically practiced in thermal desalination processes is also adopted for the MD process. The idea is to enhance the single-pass recovery ratio and hence the specific energy consumption. Thereby, numerous investigations highlighted the usage of cascading in the MD process [15,31,58–61]. In these studies, various structures such as a modular unit that combine all stages in one or multiple independent units attached in either series, parallel, or series/parallel arrays were proposed. The conception is exploiting the remaining thermal energy in the outlet brine or permeate to obtain high energy retrieval. However, these multistage systems encompass a substantial number of successive MD modules which boost the overall implied surface area and consequently the capital and operation investments. Furthermore, some of these systems incur extra external energy to preheat the interstage streams which in turn soars the operating costs.

According to the aforementioned investigations, room for further improvement of the MD reliability and efficiency still exists. Therefore, the objective of this work falls in this line, that is, further studying the MD process to reveal more of its characteristics and operational capability. Thus, this effort along with others may promote the large-scale commercialization of MD in the desalination industry. Specifically, the effect of operating the MD at a fixed temperature difference but with varying inlet temperatures for both the hot and cold streams will be studied here. Almost all existing studies focus on the effect of varying the inlet hot temperature at a fixed low inlet cold temperature. The impact of the cooling water temperature, in particular, is not well addressed and not clarified in the previous studies on MD process. Specifically, three different sets of fixed inlet temperature difference at the same range of inlet hot temperature will be tested. The investigation will be carried out experimentally. Up to the author's knowledge, no such tests and associated results have been published. Usually, auxiliary cold water is used as the condenser stream. Since the auxiliary water is available at different temperatures in a typical industrial plant, the outcome of theses test helps studying its effect on the MD performance and how to adjust the corresponding hot temperature to obtain a similar reasonable water production. Such a situation may optimize the MD operation and reduce the need for additional auxiliary cooling requirements and/or heating demands.

2. DCMD process

To facilitate understanding of the MD performance results to be presented later in this work, the following brief description of its design and operation is given. The MD module is depicted in Fig. 1. The hot water solution penetrates the module on one side with a high temperature $T_{h_{in}}$. As the hot stream passes through the membrane it incompletely evaporates due to temperature differences. Because of evaporation and heat transfer to the cold side, the hot

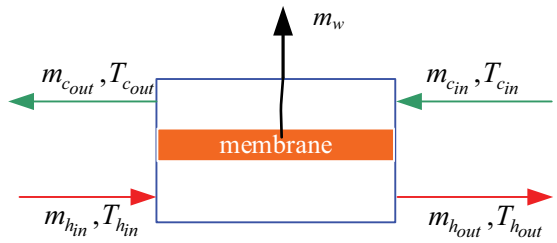

Fig. 1. Schematic of the membrane module.

solution cools down and leaves the MD with a lower temperature $T_{h_{out}}$. The water vapor transfer through the membrane's hydrophobic pores to the opposite side. On the opposite side, a cold-water stream with temperature $T_{c_{in}}$ is fed to the module in a counter-current pattern. Cold water is also known as the condenser stream because it condenses the water vapor and absorbs heat while passing through the membrane. The condenser stream warms gradually and exits at a relatively higher temperature $T_{c_{out}}$. In the literature, the cold stream is also denoted as permeate or distillate while the hot stream as feed or brine. These notions will also be used exchangeable here except the phrase "brine" will be solely for the outlet hot stream. The feed and permeate streams flow on different sides (channels) but they contact at the membrane interface. The distillate product (condensed vapor) merges with the cold stream and gets separated as fresh water. For simplicity, in Fig. 1, the distillate product (m_w) is shown to leave the module separately. In the pilot plant (Fig. 2), the distillate is collected as overflow of the cold tank and measured by electronic balance. Although the analysis in this study is based on experimental results, it is of interest to highlight the underlying physics of the process which enables the understanding of its behavior and performance. The distillate production is the mass flux multiplied by the membrane surface area. The mass flux itself occurs due to the difference between the vapor pressures at the membrane interfaces as given by Eq. (A1) listed in Appendix A. The vapor pressure difference depends on the membrane interface temperatures, T_{h_m}, T_{c_m} on the hot and cold sides, respectively. T_{h_m}, T_{c_m} are determined by solving iteratively the energy balances [Eqs. (A8) and (A9)] along with the other associated relationships listed in Appendix A. Because the paper is not modeling oriented, the model is summarized and lumped in Appendix A.

For comparison purposes, energy performance indicators will be utilized. The energy efficiency for MD is defined as the ratio of the latent heat of vaporization to the total heat consumed by the system [62], theoretically, when environmental heat losses are ignored, the thermal efficiency based on the hot stream can also be calculated as follows:

$$\mathrm{EE}_h = \frac{m_w H_v}{Q_T} \times 100 = \frac{m_w H_v}{m_h C_p \left(T_{h_{in}} - T_{h_{out}}\right)} \times 100 \tag{1}$$

where Q_T is the sensible heat lost from the hot stream while passing through the MD module, m_h is the mass rate of the hot stream, $T_{h_{in}}$ in the hot stream temperature entering the MD, and $T_{h_{out}}$ is the hot stream temperature exiting the MD module. In this sense, Q_T is the amount of heat transferred from the hot side to the cold by conduction and evaporation. Hence, the fraction of this energy utilized to vaporize the water represent the thermal efficiency of the MD module. In addition to the energy efficiency, the cooling and heating energy consumptions will also be used as performance metrics. The cooling energy demand is thus the amount of energy removed from the warm permeate stream leaving the MD module by an external heat exchanger. To avoid the use of an excessive amount of the condenser stream, the circulating condenser stream (warm permeate) is cooled down and recycled to the MD. Therefore, cooling energy depends on the outlet temperature of the stream, $T_{c_{out}}$. The cooling energy is simply the sensible heat required to cool the condenser stream from its current temperature to the desired inlet temperature. The current temperature is taken here as the temperature of the liquid inside the condenser tank. If not heat recovery is utilized, the temperature of the condenser tank is $T_{c_{out}}$ otherwise it equals the temperature of the permute leaving the heat recovery system which is dented as $T_{c_{HR}}$. Since the heat recovery system is used, the cooling energy consumption and the specific cooling energy consumption is defined as follows:

$$\mathrm{SEC}_c = \frac{\mathrm{EC}_c}{m_w} = \frac{m_c C_p \left(T_{c_{HR}} - T_{c_{in}}\right)}{m_w} \tag{2}$$

where $T_{c_{HR}}$ is the condenser stream temperature in the condenser tank, which can be calculated by solving the energy balance around the heat recovery system or measuring the temperature of the condenser tank. On the other hand, the hearing energy is the amount of heat added to the feed stream before entering the MD module using an external heat exchange. Therefore, the heating energy consumption and the specific heating energy consumption to bring the feed stream to the desired top temperature can be found as follows:

$$\mathrm{SEC}_h = \frac{\mathrm{EC}_h}{m_w} = \frac{m_c C_p \left(T_{h_{in}} - T_{h_{HR}}\right)}{m_w} \tag{3}$$

where $T_{h_{HR}}$ is the temperature of the feed stream leaving the heat recovery system. In the pilot plant, the heating energy supplied electrically. However, in this paper we consider it as energy that can be supplied from any source. Nevertheless, the heating energy consumption will be assessed for demonstration and comparison purposes. Moreover, the heating energy consumption is affected by the inlet cold temperature because heat recovery stem is utilized. SEC will be a useful comparison indicator in this study since different values for $T_{c_{in}}$ will be tested. Similarly, EE_h will be another appropriate comparison tool for the same reason besides that both $T_{c_{out}}$ and $T_{h_{out}}$ will vary accordingly.

2.1. MD experimental setup

In this study, the MD performance is investigated by running experiments using a Pilot Plant Manufactured

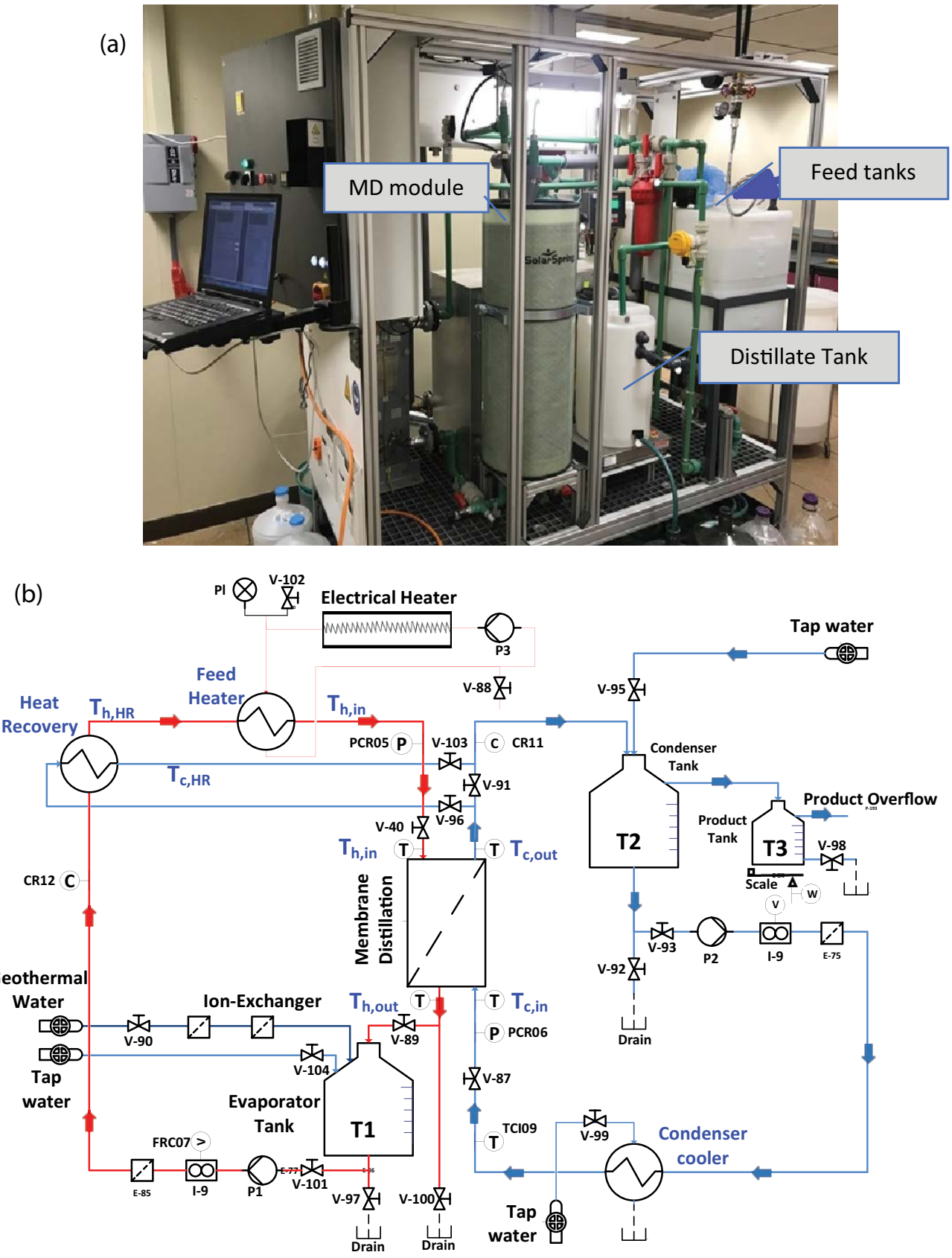

Fig. 2. (a) Photograph of the experimental rig. (b) Schematic diagram of the module test facility (flowsheet).

by SolarSpring. The plant is fitted with a DCMD module of 10 m² effective membrane-area, 230 μm thickness of the membrane, 14 m channel-length, 0.7 m channel-height, 0.2 μm pore diameter, and 2 mm channel-gap. The membrane porosity is 0.8 and the water entry pressure is 4.1 bar. A programmable logic controller (PLC) is employed for control and data logging of the DCMD unit. The human-machine-interface (HMI) is provided via a webserver. The pilot plant has been fully described and intensively used in previous works [63–65]. The reliability of the pilot plant outcomes is also compared to published data [64,65].

Fig. 2a depicts the picture of the experimental rig. Fig. 2b describes the process flow sheet of the pilot plant. Two major hydraulic flow circuits are outlined. The evaporator circuit (hot stream) is pumped from and to the water evaporator tank which contains the saline water. The volumetric flow rate of the evaporator circuit can be varied between 0 and 700 L/h which corresponds to Reynold number between 0 and 1,522. The temperature of the evaporator stream can be adjusted up to 80°C using an electrical heater that supplies the required heat duty to the heat exchanger H1. The condenser circuit (cold stream) is circulated from and to the condenser tank which is filled with distillate water having pH around 7. Both the temperature and volume flow rate of the two circuits is controlled over PLC. The volume flow rate of the cold stream is maintained equal to that of the hot circuit. Note the DCMD module does not permit operating with uneven flow rates for the hot and cold streams to prevent distortion of the membrane material. The heat exchanger (H2) is used to control the condenser stream temperature using a cold-water stream in the cooling loop. The heat exchanger (H3) is responsible for heat recovery (HR) which can be activated by adjusting valves (A.005, A.007, and A.009). The potable water is withdrawn from the condenser circuit by an overflow, collected, and measured in the product tank. All process measurements are forecasted via HMI and stored in a PC for further utilization.

3. Experimental procedure

All the result data to be shown and analyzed in this work is generated from experimental runs. For all experiments, the volume flow rate for both circuits is fixed at 300 L/h, equivalent to Reynolds number of 561. The hot stream has a salinity of 1,000 mg/L to resemble brackish water. The MD setup will be tested for three fixed cross-temperature differences of 30°C, 40°C, and 50°C. By cross-temperature difference, we mean the temperature difference between the inlet's hot and cold temperatures. For each fixed temperature difference, different sets of inlet hot and cold temperatures are tested. Those sets are spaced by 5°. Note that for each inlet temperature set, the difference between the two inlet temperatures is kept constant. Automatic control systems are employed to keep the inlet temperatures within the set point. Those experimental tests are run till the outlet temperature reaches a steady state. Usually, the time to steady state varies with flow rate and operating temperature. The experiments are run for longer time (2~3 h) to ensure reaching steady state. The measurements at the end of the experiment are taken as the steady state value. At the steady state, the water mass production rate is estimated from the accumulated water mass production. It should be noted that the standard deviation of the temperature measurements ranges between ±0.31°C and ±0.65°C with an uncertainty of 0.02°C~0.04°C. For the flow rate measurements, the standard deviation ranges between ±2.88 to ±12.1 L/h with an uncertainty of 0.2~0.8 L/h. The standard deviation in the measurements of the accumulated water mass is ±3.33 kg with an uncertainty of 0.22 kg.

Fig. 3 shows an example of the typical results of an experimental run at a fixed temperature difference of 40°C. In this case, the inlet hot temperature is set to 55°C, and the cold temperature is 15°C. The inlet hot temperature is regulated by the built-in PLC system while the inlet cold temperature is controlled by a local digital temperature controller. Fig. 3a displays the temperature response. The experiment starts at room temperature. The temperatures undergo transient behavior for the first 15~20 min till they reach a steady state. Fig. 3b depicts the response of the accumulated water mass production. Note that the produced water builds up with time and hence behaves as a straight line. This ramp function is then differenced with time to obtain the water mass production rate. Alternatively, the slope of the straight line resembles the production rate. This experimental run is repeated for several coordinated inlet temperatures at different fixed cross-temperature differences as mentioned earlier. It should be noted that the inlet cold temperature, $T_{c_{in}}$ is physically restricted between 15°C and 40°C. An inlet cold temperature higher than 40°C is not permissible in this experimental setup. The MD module is designed such that it automatically shut down when $T_{c_{in}}$ exceeds 40°C to avoid overheating the system. On the other hand, an inlet

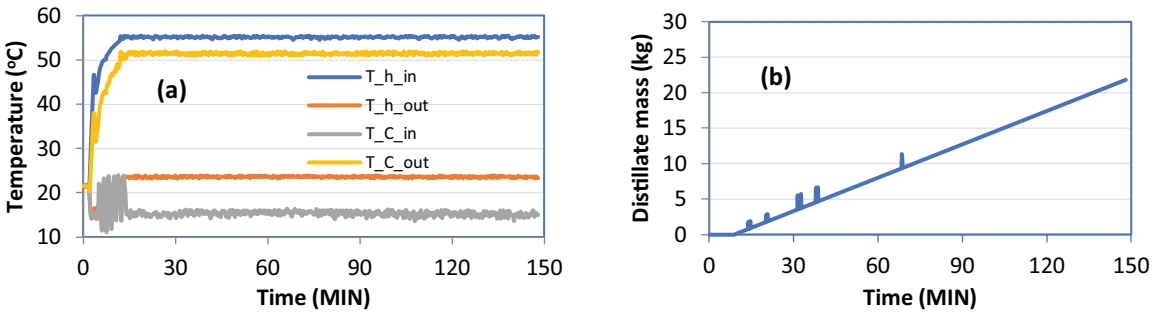

Fig. 3. Sample of experimental run; $dT = 40°C$, $T_{h_{in}} = 55°C, T_{c_{in}} = 15°C$.

cold temperature less than 15°C is not possible because of the limitation of the cooling system. Similarly, the maximum inlet hot temperature, $T_{h_{in}}$ is bounded by 80°C due to the capacity of the heating system. The analysis of experimental tests is summarized in the following section.

4. Results and discussion

4.1. Temperature profile

This section demonstrates and analyses the measured temperature profile obtained from experimental test carried out at fixed cross temperature difference. The range of parameters for the experimental test is listed in Table 1. Fig. 4 summarizes the results of the experimental runs for three selected temperature differences, that is, dT = 30°C, 40°C, and 50°C. In each case of fixed dT, different pairs of ($T_{h_{in}}$, $T_{c_{in}}$) are examined. The range of examined $T_{h_{in}}$ is controlled by the upper and lower bounds on $T_{c_{in}}$ and the upper bound on $T_{h_{in}}$ mentioned previously. For example, Fig. 4a, which is devoted for dT = 30°C, the inlet hot temperature ranges between 45°C and 70°C, because it is limited by the lower and upper bounds on $T_{c_{in}}$, respectively. Fig. 4b is devoted for dT = 40°C, hence the inlet hot temperature ranges between 55°C and 80°C, because it is restricted by the lower bound on $T_{c_{in}}$ and the upper bound on both $T_{h_{in}}$, respectively. Similarly, Fig. 4c, which is devoted for dT = 50°C, the inlet hot temperature ranges between 65°C and 80°C, because it is restricted by the lower bound on $T_{c_{in}}$ and the upper bound on both $T_{h_{in}}$, respectively. Note that in all these tests, the paired inlet temperatures are fixed by the controller and the resulted outlet temperatures, that is, $T_{h_{out}}$, $T_{c_{out}}$ are recorded at steady state. The value of the outlet temperatures is the outcome of the MD heat and mass operations induced by the paired inlet temperatures. Interestingly, the permeate outlet temperature changes uniformly and consistently for all tested dT's. In fact, the profile of the permeate outlet temperature is almost parallel to the inlet hot temperature and within 2°~3° difference. This is intuitive because as the input thermal energy increases, the temperature of the permeate will increase accordingly, that is, $T_{c_{out}}$ follows the trend of $T_{h_{in}}$. Moreover, it also means that the trend of $T_{c_{out}}$ for all cases of dT is insensitive to the applied fixed temperature difference. For a counter-current regime and equal flow rate for the feed and cold stream, higher energy efficiency and hence uniform temperature distribution can be obtained [16]. On the other hand, the profile of the outlet feed temperature exhibits variation with dT and $T_{h_{in}}$. Usually, due to conduction, convection, and heat losses, the feed stream leaves the unit at a very low outlet temperature. The alteration of the outlet feed temperature with $T_{h_{in}}$ is very likely because as the feed enters at a higher temperature, it will depart the system correspondingly with relatively a higher degree. Although the outlet hot temperature varies with dT, its distance from $T_{h_{in}}$ remains consistent for all dT's and tested inlet temperatures. For dT = 30°C and 40°C, because high values of $T_{c_{in}}$ (>30°C) is used at high values of $T_{h_{in}}$ the outlet hot temperature approaches the inlet cold temperatures. For comparison purposes and better visualization of the effect of dT on the outlet temperatures, the latter are grouped and plotted in one graph as shown in Fig. 5. Clearly, as discussed earlier the profile of the outlet permeate temperature is insensitive to dT as all the corresponding trends coincides. However, the profile of the outlet feed temperature changes inversely with dT. For example, the outlet temperature has the lowest values at dT = 50°C. In this case, the inlet cold temperature profile has a lower value than that of the other dT's for the sample operating top temperature. This situation induces higher heat transfer between the hot and cold channels. As a result, the brine will leave the MD at lower temperature. Further analysis and discussion of the obtained temperature profiles will continue in the next section using differenced data.

Table 1
Range of parameters for the experimental tests

Mass flow rate	dT = 30°C		dT = 40°C		dT = 50°C		$T_{c_{in}}$ = 15°C	
	$m_{h_{in}} = m_{c_{in}}$ = 300 L/h							
	$T_{c_{in}}$	$T_{h_{in}}$	$T_{c_{in}}$	$T_{h_{in}}$	$T_{c_{in}}$	$T_{h_{in}}$	$T_{c_{in}}$	$T_{h_{in}}$
Test 1	15	45	15	55	15	65	15	45
Test 2	20	50	20	60	20	70	15	50
Test 3	25	55	25	65	25	75	15	55
Test 4	30	60	30	70	30	80	15	60
Test 5	35	65	35	75			15	65
Test 6	40	70	40	80			15	70
Test 7							15	75
Test 8							15	80

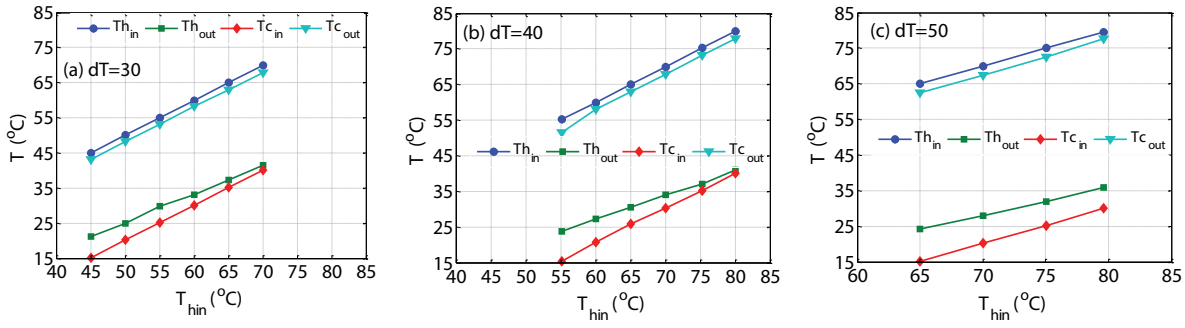

Fig. 4. Membrane distillation inlet and outlet temperature measurements for (a) dT = 30°C, (b) dT = 40°C, and (c) dT = 50°C.

The measured temperatures shown in Fig. 4 are differenced and replotted in Fig. 6 for demonstration purposes. Specifically, Fig. 6a shows the differenced temperature of the feed stream, that is, $dT_h = T_{h_{in}} - T_{h_{out}}$, Fig. 6b shows the differenced temperature of the cold stream, that is, $dT_c = T_{c_{out}} - T_{c_{in}}$, and Fig. 6c shows the differenced temperature of the outlet streams, that is, $dT_{out} = T_{c_{out}} - T_{h_{out}}$. The temperature drop at the feed side (dT_h) is a manifestation of the heat supplied by the feed stream and subsequently reflects the extent of the mass and heat transfer activities. For all tested temperature differences, dT_h increases with the inlet feed temperature although the inlet temperature difference is fixed (Fig. 6a). The increment of dT_h is an indication of improved mass and heat transfer activities which is the direct consequences of increasing $T_{h_{in}}$. High inlet feed temperature enhances the film heat transfer coefficient which reduces the heat transfer resistance. In addition, dT_h becomes larger at larger dT which is a direct consequence of the results shown in Fig. 5. Smaller values for the outlet feed temperature at dT = 50°C (Fig. 5) will of course lead to a larger dT_h profile as shown in Fig. 6a. The temperature drop at the cold side (dT_c) shows an interesting trend as shown in Fig. 6b. The trends with respect to $T_{h_{in}}$ are almost constant except for dT = 40°C where the trend is slightly changing. Again, this is a direct reflection of the profile of $T_{c_{out}}$ shown in Fig. 5 where the rate of change was constant around 1. Nevertheless, dT_c has a larger magnitude at the largest dT because the corresponding inlet cold temperature is relatively smaller than the other cases. Remarkably, dT_c possesses a larger value than dT_h which requires additional investigation. Finally, Fig. 6c displays the projection of dT_{out} which represents the extent of separation activities as a wider value means improved heat transfer. Idealistically dT_{out} should be constant for each fixed dT. However, the separation mechanism is complex and strongly affected by the magnitude of the bulk temperatures. Obviously, dT_{out} becomes wider at higher inlet feed temperature and greater dT. The rate of increment of dT_{out} with inlet feed temperature is small but slightly higher at dT = 40°C. The effect of the inlet feed temperature on dT_{out} is straightforward as mentioned earlier. The effect of dT on dT_{out} is also obvious which is a direct consequence of the results shown in Fig. 5. Nevertheless, the best performance in terms of improved thermal efficiency due to improved heat transfer occurs at the highest dT and $T_{h_{in}}$.

4.2. Mass flux profile and analysis

The important parameter of the MD process is the distillate production manifested by the water mass flux. The implication of the proposed experimental tests on the water mass flux will be analysed in this section. The water flux that corresponds to the tests given in Fig. 4 is illustrated in Fig. 7. It was expected that since the inlet temperature difference is fixed, the driving force will also be constant leading to a fixed water production regardless of the value of $T_{h_{in}}$.

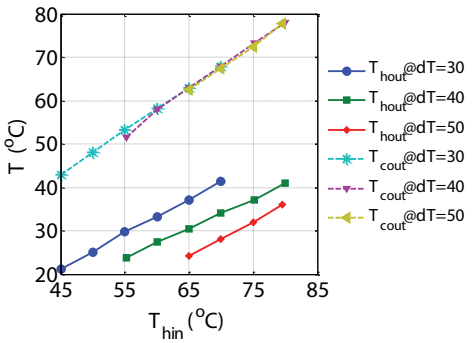

Fig. 5. $T_{c_{out}}$ and $T_{h_{out}}$ measurements for the three fixed temperature differences.

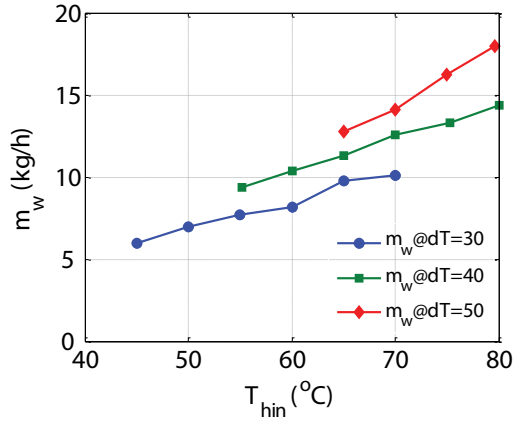

Fig. 7. Water production for the three selected temperature differences.

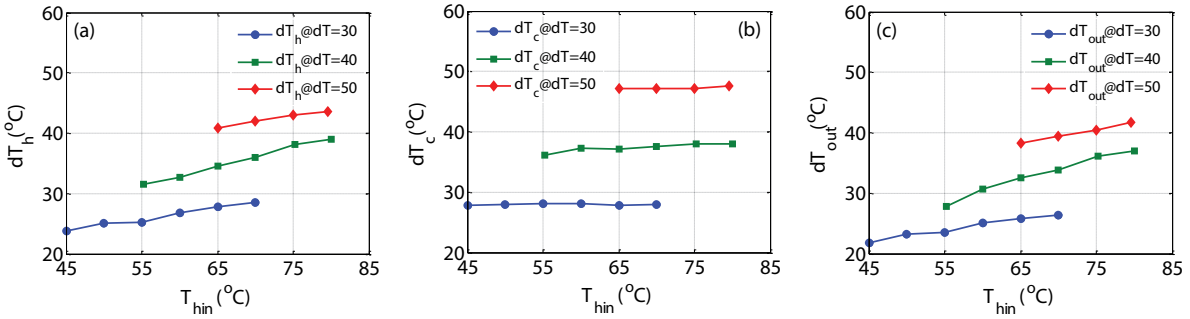

Fig. 6. Temperature differences for the three cases, (a) $dT_h = T_{h_{in}} - T_{h_{out}}$, (b) $dT_c = T_{c_{out}} - T_{c_{in}}$, and (c) $dT_{out} = T_{c_{out}} - T_{h_{out}}$.

Interestingly, the obtained water mass production increases with $T_{h_{in}}$ although the temperature difference is fixed. This indicates that $T_{h_{in}}$ has a prominent impact on the MD performance in terms of water mass production. In fact, the mass flux is proportional to the temperature difference at the membrane interface. However, the latter was expected to be also constant as it is correlated to the inlet temperature difference. It turns out that the effect of $T_{h_{in}}$ prevails because higher $T_{h_{in}}$ will promote evaporation and enhance the film heat transfer coefficient in the hot channel. The improved heat transfer will reduce the heat transfer resistance in the hot channel resulting in a higher value for T_{h_m}, that is, the hot temperature at the membrane interface. This situation widens the difference between T_{h_m} and T_{c_m}, in another word reduces the temperature polarization effect, causing higher vapor pressure difference and consequently larger mass flux rate. It should be remembered that the vapor pressure varies exponentially with temperature. Hence even if the temperature difference is fixed, the vapor pressure will still propagate. On the other hand, the water flux increases with dT which is intuitive. The larger temperature difference will also cause a wider temperature difference at the membrane interface as they are correlated. This situation will also enlarge the vapor pressure difference and consequently the vapor flux. To assess the effect of $T_{h_{in}}$ on the gained mass flux, the ratio of mass flux gain to the increase in $T_{h_{in}}$ is calculated. Note the gained mass flux is normalized by the feed temperature because the range of applied $T_{h_{in}}$ is different in the three cases. The rate of change is 0.36, 0.2, and 0.16 kg/h per °C for dT = 50°C, 40°C, and 30°C, respectively. This corresponds to 25% and 125% increase when increasing dT from 30°C to 40°C and 50°C, respectively. To assess the effect of dT, we compare the water flux at an inlet feed temperature of 65°C. At this operating top temperature, the water production at dT = 50°C is 13% and 30% higher than that of dT = 40 and 30°C, respectively. At an inlet feed temperature of 80°C, the water production of dT = 50°C is 25% higher than that of dT = 40°C.

Regardless of the variable performance of the MD systems with the tested operating conditions, the results shown in Fig. 7 confirmed the possibility of producing high fresh water even when the inlet cold temperature is as high as 30°C or even 40°C. This is an attractive feature because it eliminates the need for subcooled condenser water. This leads to saving on the cost of cooling. Usually, auxiliary water at a temperature of less than 25°C is seldom available and hence additional cooling energy is required to provide such low-temperature auxiliary water. Even if such auxiliary water is available at low temperatures, it is still costly. If the auxiliary water must be recycled to the MD after use, then it requires re-cooling because it gets heated when leaving the MD unit. If the auxiliary water will not be recycled, then a huge amount of condenser stream will be consumed equivalent to the amount of saline water to be treated.

4.3. Testing MD for fixed inlet cold temperature

To further assess the benefit of the use of high inlet cold temperatures we analyse the energy requirements. For constructive analysis, the energy demands of operating at fixed dT will be compared to that of operating at fixed inlet cold temperatures. For this purpose, the MD performance in terms of temperature and water production variation under fixed inlet cold temperature should be first analysed. Hence, the MD plant is retested for several values for $T_{h_{in}}$ but at a fixed value of 15°C for the inlet cold temperature, this means the inlet temperature difference is variable. The resulting projection of the measured inlet and outlet temperatures is displayed in Fig. 8a. Obviously, the gap between $T_{h_{in}}$ and $T_{c_{in}}$ widens rapidly because the latter is fixed. This situation enhances the heart transfer activity between the cold and hot channels causing $T_{h_{out}}$ to exit the unit at low temperature. In this case, $T_{h_{out}}$ does not grow proportionally with $T_{h_{in}}$ as the case when dT is fixed as shown in Fig. 4. Moreover, the widening gap between $T_{h_{in}}$ and $T_{c_{in}}$ will consequently broaden the driving force generating more mass flux as depicted in Fig. 8b. Indeed, the water production at a fixed inlet cold temperature of 15°C grows linearly and rapidly with $T_{h_{in}}$ which surpasses the water production of the other cases of fixed dT as shown in Fig. 8b. Interestingly, the water production at a fixed inlet cold temperature of 15°C matches that of the other cases at specific conditions, that is, when dT has the same value. For example, it matches that of dT = 30°C at $T_{h_{in}}$ = 45°C of dT = 40°C at $T_{h_{in}}$ = 55°C, and of dT = 50°C at $T_{h_{in}}$ = 65°C. This affirms the reproducibility of the experimental results. Evidently and expectedly, it is beneficial to operate at low inlet cold temperatures. However, the main goal of testing the MD at fixed inlet cold temperature is to examine its

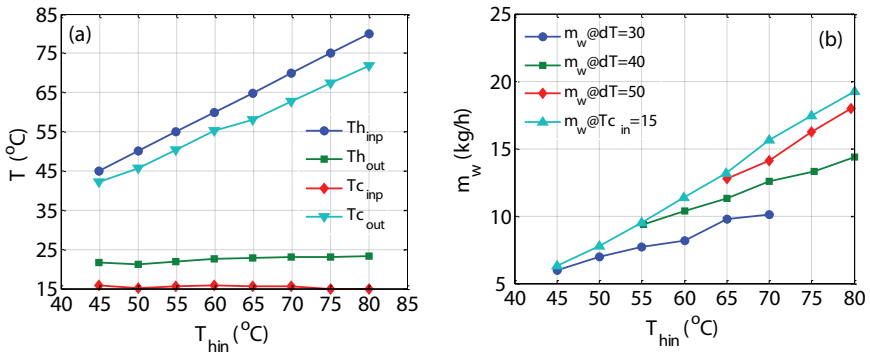

Fig. 8. Comparison of water production for the three selected temperature differences with water production at fixed inlet temperature of 15°C; (a) temperature profile for fixed inlet temperature of 15°C and (b) water production comparison.

impact on the energy demands as will be discussed in the next section.

4.4. Energy consumption analysis

In this section, comparison between the operation at fixed dT and at fixed inlet cold temperature will be analysed based on the energy consumption. Fig. 9 demonstrates the cooling energy and specific energy consumption. Fig. 9a shows how the cooling energy requirement for fixed $T_{c_{in}}$ evolves rapidly with the inlet feed temperature. According to Fig. 8a, the outlet temperature of the permeate grows proportionally with $T_{h_{in}}$ and hence the required energy to cool the permeate stream down to 15°C surges. Consequently, the cooling energy demand for operating at fixed $T_{c_{in}}$ exceeds that for operating at fixed temperature difference. The cooling energy requirements for fixed dT decrease slightly with the inlet feed temperature. According to Fig. 6b, the cooling energy demand should be constant over $T_{h_{in}}$ as dT_c is constant. However, since the recovery system is involved, the permeate temperature departing the heat recovery decreases because the outlet feed temperature increases as shown in Fig. 5. Moreover, the energy of cooling enlarges for larger dT. This is a direct consequence of the results shown in Fig. 6b. Since the production rate increases for both fixed dT and fixed $T_{c_{in}}$ but at different rates, the corresponding specific energy consumption of cooling will decrease at different rates as depicted in Fig. 9b. In this case, SEC_c for fixed inlet cold temperature becomes comparable to the other cases except at $T_{h_{in}} = 80$°C where it becomes the worst. Thereby, SEC for cooling does not pose a serious challenge for fixed $T_{c_{in}}$ compared to fixed dT, or more specifically at low $T_{c_{in}}$ compared to high $T_{c_{in}}$ However, it should be remembered that the use of auxiliary cooling water at temperatures higher than 25°C is considered free of the cost compared to 15°C.

Fig. 10 illustrates the heating energy and the specific heating energy consumption. Evidently, operating at fixed $T_{c_{in}}$ incurs large and rapidly growing heating energy as shown in Fig. 10a. The escalating heating demand is evident from the soaring difference between $T_{h_{in}}$ and $T_{h_{out}}$ shown in Fig. 8a. The heating energy for fixed dT grows with inlet feed temperature but at a very smaller rate. The reason for the slowly increasing heating demand is the corresponding growing value of $T_{h_{out}}$ shown in Fig. 5. The heating energy for fixed dT remains lower than that for fixed $T_{c_{in}}$. This is ascribed to the difference in magnitude of their corresponding $T_{h_{out}}$ shown in Figs. 5 and 8a and the effect of the recovery system. Note that the heating energy is computed using $T_{h_{HR}}$ which is higher than and directly proportional to $T_{h_{out}}$. This makes the recovery system and particularly the value of $T_{c_{in}}$ influences the heating energy demand. For example, as shown in Fig. 8, for low fixed inlet cold temperature, the corresponding outlet permeate temperature is relatively lower than that for fixed dT shown in Fig. 5. Accordingly, the effectiveness of the recovery system is lesser leading

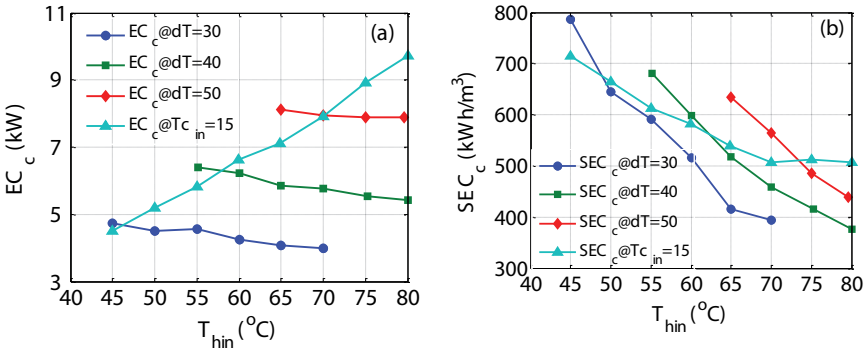

Fig. 9. Cooling energy requirements for the three selected temperature differences and fixed inlet temperature of 15°C, (a) energy consumption and (b) specific energy consumption.

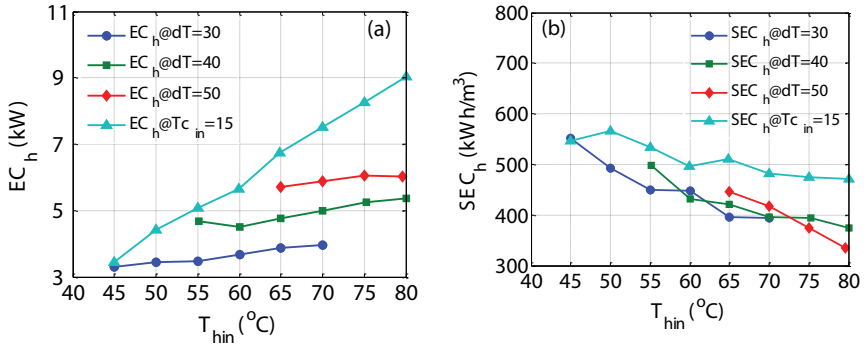

Fig. 10. Heating energy requirements for the three selected temperature differences and fixed inlet temperature of 15°C, (a) energy consumption and (b) specific energy consumption.

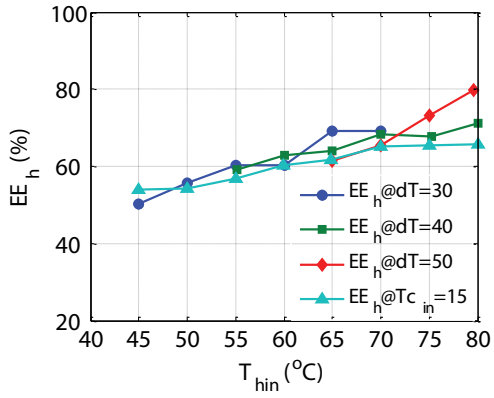

Fig. 11. Energy efficiency for the three selected temperature differences and fixed inlet cold temperature of 15°C.

to lower value for $T_{h_{HR}}$ and subsequently higher heating energy demand. Another important observation is that the heating energy demand is much less than the cooling energy demand. Of course, this is due to the use of heat recovery system, but the cooling energy remains an issue that overlooked by many researchers. Most of the published investigations is concerned with the heating energy although it can be alleviated by recovery system and utilization of low-grade heat sources. The specific energy consumption for heating is compared in Fig. 10b. For all cases, the specific heating requirements decrease with inlet feed temperature as expected because their corresponding water production increases with temperature. Indeed, the specific energy consumption for operating at low fixed $T_{c_{in}}$ exceeds that for fixed dT over the entire operating top temperature except at 45°C. At the optimum top temperature of 80°C, SEC_h for $T_{c_{in}} = 15°C$ is 40% higher than that for $dT = 50°C$. Accordingly, operating at fixed dT becomes superior to that for fixed $T_{c_{in}}$.

Lastly, we compare the energy efficiency of the MD for all cases as shown in Fig. 11. The process delivered comparable efficiency for the different cases with the efficiency ranges between 50% at the lowest tested temperature and 70%~80% at the maximum tested temperature. Typically, heat loss from the feed due to latent heat transfer grows with temperature improving MD efficiency. Swaminathan et al. [16] reported an energy efficiency of about 40% while Gilron et al. [66] reported an efficiency of 60%. Anyway, operating at low fixed $T_{c_{in}}$ exhibits slightly lower energy efficiency than the other cases. At the same highest top temperature, the energy efficiency when operating at $dT = 50°C$, that is, $T_{c_{in}} = 30°C$ outperforms that operating at $T_{c_{in}} = 15°C$ by 21%.

5. Conclusions

MD plant is tested for operation under coordinated varying inlet temperatures at a fixed distance. Based on the plant design capacity, three fixed inlet temperature differences were examined, for example, 30°C, 40°C, and 50°C. It is found that a larger inlet temperature difference improves water production because it maximizes the driving force and consequently the vapor flux through the porous membrane. It is also found that increasing the inlet feed temperature at a fixed inlet temperature difference promotes more mass flux, decreases specific energy consumption, and enhances the membrane's thermal efficiency. Hence, the top brine temperature is a vital design parameter that effectively influences the MD performance. Operating at fixed inlet temperature difference revealed that using relatively higher inlet cold temperatures can still provide excellent performance, especially in terms of energy effectiveness. At the same highest top temperature of 80°C, using an inlet cold temperature of 30°C can outperform that using an inlet cold temperature of 15°C in the sense of less cooling energy consumption, lower heating energy consumption, and higher thermal efficiency. In fact, operating at relatively high inlet cold temperatures eliminates the need for cooling energy as auxiliary wastewater is widely available in industrial plants.

Acknowledgment

This project is funded by the Researchers Supporting Project number (RSP2023R510), King Saud University, Riyadh, Saudi Arabia.

Symbols

A_s	—	Surface area, m²
A	—	Cross-sectional area, m²
C_m	—	Permeability coefficient, kg/m²·s·Pa
C_m^k	—	Knudsen mass flux coefficient, kg/m²·s·Pa
C_m^d	—	Molecule diffusion mass flux coefficient, kg/m²·s·Pa
C_m^c	—	Transition mass flux coefficient, kg/m²·s·Pa
C_p	—	Heat capacity, J/kg·K
C_s	—	Salt concentration, %
d	—	Hydraulic diameter, m
EC_c	—	Cooling energy consumption, kJ/h
EC_h	—	Heating energy consumption, kJ/h
H_v	—	Latent heat of vaporization, J/kg
H_{loss}	—	Heat loss, kW
h_f, h_p, h_m	—	Feed, permeate, and membrane heat transfer coefficient, W/m²·K
h	—	Membrane channel height, m
J_w	—	Mass flux, kg/m²·h
k_m	—	Membrane conductivity, W/m·K
k	—	Cell (control volume) number
L	—	Membrane length, m
M_w	—	Molecular weight of water, g/mol
m_h, m_c	—	Brine (feed), cold (permeate) flow rates, respectively, kg/h
$m_{h_{in}}$, $m_{h_{out}}$	—	Inlet and outlet hot feed flow rate, respectively, kg/h
$m_{c_{in}}$, $m_{c_{out}}$	—	Inlet and outlet cold stream flow rate, respectively, kg/h
m_w	—	distillate flow rate, kg/h
Nu	—	Nusselt number
n	—	Number of divisions (cell) of the membrane length
ns	—	Number of stages
nsc	—	Number of sections
P_1, P_2	—	Vapor pressure at feed and permeate membrane surface, Pa
PD	—	Membrane pressure multiplied by diffusivity, Pam²/s

P_a	—	Entrapped air pressure, Pa
Pr	—	Prandtl number
q_f, q_p	—	Heat transfer rate at feed and permeate sections, W/m^2
q_m	—	Heat of evaporation and conduction, W/m^2
q_t	—	Overall heat flux, W/m^2
Q_T	—	Sensible heat of the feed stream, kJ/h
r	—	Pore size, m
R	—	Ideal gas constant, J/mol·K
SEC_c	—	Specific cooling energy consumption, kW·h/m^3
SEC_h	—	Specific heating energy consumption, kW·h/m^3
Re	—	Reynold number
T	—	Average temperature, K
T_h, T_c	—	Feed (hot) and permeate (cold) bulk temperature, K
T_{hm}, T_{cm}	—	Feed and permeate temperature at membrane surface, K
$T_{h_{out}}$, $T_{h_{in}}$	—	Outlet and inlet hot feed temperature, °C
$T_{c_{out}}$, $T_{c_{in}}$	—	Outlet and inlet cold stream temperature, °C
$T_{c_{HR}}$	—	Permeate temperature leaving the heat recovery system, °C
$T_{h_{HR}}$	—	Feed temperature leaving the heat recovery system, °C
U	—	Overall heat transfer coefficient, W/m^2·K

Greek letters

ε	—	Porosity
τ	—	Membrane tortuosity
δ	—	Membrane thickness, mm
ρ	—	Density, kg/m^3
Δ	—	Difference operator

References

[1] B.R. Bodell, Silicone Rubber Vapor Diffusion in Saline Water Distillation, US Patent 285,032, 1963.

[2] R. Schwantes, K. Chavan, D. Winter, C. Felsmann, J. Pfafferott, Techno-economic comparison of membrane distillation and MVC in a zero liquid discharge application, Desalination, 428 (2018) 50–68.

[3] A. Alkhudhiri, N. Darwish, N. Hilal, Membrane distillation: a comprehensive review, Desalination, 287 (2012) 2–18.

[4] A.M. Alklaibi, N. Lior, Transport analysis of air-gap membrane distillation, J. Membr. Sci., 255 (2005) 239–253.

[5] J. Chang, J. Zuo, K.-J. Lu, T.-S. Chung, Membrane development and energy analysis of freeze desalination-vacuum membrane distillation hybrid systems powered by LNG regasification and solar energy, Desalination, 449 (2019) 16–25.

[6] O.R. Lokare, S. Tavakkoli, S. Wadekar, V. Khanna, R.D. Vidic, Fouling in direct contact membrane distillation of produced water from unconventional gas extraction, J. Membr. Sci., 524 (2017) 493–501.

[7] K.J. Lu, Z.L. Cheng, J. Chang, L. Luo, T.-S. Chung, Design of zero liquid discharge desalination (ZLDD) systems consisting of freeze desalination, membrane distillation, and crystallization powered by green energies, Desalination, 458 (2019) 66–75.

[8] K.W. Lawson, D.R. Lloyd, Membrane distillation, J. Membr. Sci., 124 (1997) 1–25.

[9] Z. Zhang, O.R. Lokare, A.V. Gusa, R.D. Vidic, Pretreatment of brackish water reverse osmosis (BWRO) concentrate to enhance water recovery in inland desalination plants by direct contact membrane distillation (DCMD), Desalination, 508 (2021) 115050, doi: 10.1016/j.desal.2021.115050.

[10] A. Panagopoulos, Brine management (saline water & wastewater effluents): sustainable utilization and resource recovery strategy through Minimal and Zero Liquid Discharge (MLD & ZLD) desalination systems, Chem. Eng. Process. Process Intensif., 176 (2022) 108944, doi: 10.1016/j.cep.2022.108944.

[11] A. Panagopoulos, Techno-economic assessment of zero liquid discharge (ZLD) systems for sustainable treatment, minimization and valorization of seawater brine, J. Environ. Manage., 306 (2022) 114488, doi: 10.1016/j.jenvman.2022.114488.

[12] U.K. Kesieme, N. Milne, H. Aral, C.Y. Cheng, M. Duke, Economic analysis of desalination technologies in the context of carbon pricing, and opportunities for membrane distillation, Desalination, 323 (2013) 66–74.

[13] J. Phattaranawik, R. Jiraratananon, Direct contact membrane distillation: effect of mass transfer on heat transfer, J. Membr. Sci., 188 (2001) 137–143.

[14] E.K. Summers, H.A. Arafat, Energy efficiency comparison of single-stage membrane distillation (MD) desalination cycles in different configurations, Desalination, 290 (2012) 54–66.

[15] J.-G. Lee, W.-S. Kim, J.-S. Choi, N. Ghaffour, Y.-D. Kim, A novel multi-stage direct contact membrane distillation module: design, experimental and theoretical approaches, Water Res., 107 (2016) 47–56.

[16] J. Swaminathan, H.W. Chung, D.M. Warsinger, Simple method for balancing direct contact membrane distillation, Desalination, 383 (2016) 53–59.

[17] M. Qtaishat, T. Matsuura, B. Kruczek, M. Khayet, Heat and mass transfer analysis in direct contact membrane distillation, Desalination, 219 (2008) 272–292.

[18] S. Bandini, G.C. Sarti, Concentration of must through vacuum membrane distillation, Desalination, 149 (2002) 253–259.

[19] S. Gunko, S. Verbych, M. Bryk, N. Hilal, Concentration of apple juice using direct contact membrane distillation, Desalination, 190 (2006) 117–124.

[20] J. Grzechulska-Damszel, M. Tomaszewska, A. Morawski, Integration of photocatalysis with membrane processes for purification of water contaminated with organic dyes, Desalination, 241 (2009) 118–126.

[21] Y. Huo, Z. Xie, X. Wang, H. Li, M. Hoang, R.A. Caruso, Methyl orange removal by combined visible-light photocatalysis and membrane distillation, Dyes Pigm., 98 (2013) 106–112.

[22] A. Criscuoli, E. Drioli, A. Capuano, B. Memoli, V. Andreucci, Human plasma ultrafiltrate purification by membrane distillation: process optimisation and evaluation of its possible application on-line, Desalination, 147 (2002) 147–148.

[23] Z. Ding, L. Liu, Z. Liu, R. Ma, The use of intermittent gas bubbling to control membrane fouling in concentrating TCM extract by membrane distillation, J. Membr. Sci., 372 (2011) 172–181.

[24] N. Couffin, C. Cabassud, V. Lahoussine-Turcaud, A new process to remove halogenated VOCs for drinking water production: vacuum membrane distillation, Desalination, 117 (1998) 233–245.

[25] M. Khayet, Treatment of radioactive wastewater solutions by direct contact membrane distillation using surface modified membranes, Desalination, 321 (2013) 60–66.

[26] P. Zolotarev, V. Ugrozov, I. Volkina, V. Nikulin, Treatment of waste water for removing heavy metals by membrane distillation, J. Hazard. Mater., 37 (1994) 77–82.

[27] M. Tomaszewska, M. Gryta, A. Morawski, Study on the concentration of acids by membrane distillation, J. Membr. Sci., 102 (1995) 113–122.

[28] M. Rezaei, D.M. Warsinger, M.C. Duke, T. Matsuura, W.M. Samhaber, Wetting phenomena in membrane distillation: mechanisms, reversal, and prevention, Water Res., 139 (2018) 329–352.

[29] J. Swaminathan, H.W. Chung, D.M. Warsinger, Energy efficiency of membrane distillation up to high salinity: evaluating critical system size and optimal membrane thickness, Appl. Energy, 211 (2018) 715–734.

[30] A. Ali, J.-H. Tsai, K.-L. Tung, E. Drioli, F. Macedonio, Designing and optimization of continuous direct contact membrane distillation process, Desalination, 426 (2018) 97–107.
[31] F. He, J. Gilron, K.K. Sirkar, High water recovery in direct contact membrane distillation using a series of cascades, Desalination, 323 (2013) 48–54.
[32] D.M. Warsinger, J. Swaminathan, E. Guillen-Burrieza, H.A. Arafat, Scaling and fouling in membrane distillation for desalination applications: a review, Desalination, 356 (2015) 294–313.
[33] M. Gryta, Alkaline scaling in the membrane distillation process, Desalination, 228 (2008) 128–134.
[34] D. Hou, J. Wang, D. Qu, Z. Luan, C. Zhao, X. Ren, Desalination of brackish groundwater by direct contact membrane distillation, Water Sci. Technol., 61 (2010) 2013–2020.
[35] A. Panagopoulos, K.-J. Haralambous, Minimal Liquid Discharge (MLD) and Zero Liquid Discharge (ZLD) strategies for wastewater management and resource recovery – analysis, challenges and prospects, J. Environ. Chem. Eng., 8 (2020) 104418, doi: 10.1016/j.jece.2020.104418.
[36] J. Morillo, J. Usero, D. Rosado, H. El Bakouri, A. Riaza, F.-J. Bernaola, Comparative study of brine management technologies for desalination plants, Desalination, 336 (2014) 32–49.
[37] E. Drioli, A. Ali, S. Simone, F. Macedonio, S. Al-Jlil, F. Al Shabonah, H. Al-Romaih, O. Al-Harbi, A. Figoli, A. Criscuoli, Novel PVDF hollow fiber membranes for vacuum and direct contact membrane distillation applications, Sep. Purif. Technol., 115 (2013) 27–38.
[38] L.D. Tijing, J.-S. Choi, S. Lee, S.-H. Kim, H.K. Shon, Recent progress of membrane distillation using electrospun nanofibrous membrane, J. Membr. Sci., 453 (2014) 435–462.
[39] P. Wang, T.-S. Chung, Recent advances in membrane distillation processes: membrane development, configuration design and application exploring, J. Membr. Sci., 474 (2015) 39–56.
[40] R. Schwantes, A. Cipollina, F. Gross, J. Koschikowski, D. Pfeifle, M. Rolletschek, V. Subiela, Membrane distillation: solar and waste heat driven demonstration plants for desalination, Desalination, 323 (2013) 93–106.
[41] A. Ali, F. Macedonio, E. Drioli, S. Aljlil, O. Alharbi, Experimental and theoretical evaluation of temperature polarization phenomenon in direct contact membrane distillation, Chem. Eng. Res. Des., 91 (2013) 1966–1977.
[42] K. Zhao, W. Heinzl, M. Wenzel, S. Büttner, F. Bollen, G. Lange, S. Heinzl, N. Sarda, Experimental study of the memsys vacuum-multi-effect-membrane-distillation (V-MEMD) module, Desalination, 323 (2013) 150–160.
[43] L. Francis, N. Ghaffour, A.A. Alsaadi, G.L. Amy, Material gap membrane distillation: a new design for water vapor flux enhancement, J. Membr. Sci., 448 (2013) 240–247.
[44] H.C. Duong, P. Cooper, B. Nelemans, T.Y. Cath, L.D. Nghiem, Optimising thermal efficiency of direct contact membrane distillation by brine recycling for small-scale seawater desalination, Desalination, 374 (2015) 1–9.
[45] G. Guan, X. Yang, R. Wang, A.G. Fane, Evaluation of heat utilization in membrane distillation desalination system integrated with heat recovery, Desalination, 366 (2015) 80–93.
[46] O.R. Lokare, S. Tavakkoli, V. Khanna, R.D. Vidic, Importance of feed recirculation for the overall energy consumption in membrane distillation systems, Desalination, 428 (2018) 250–254.
[47] C. Charcosset, A review of membrane processes and renewable energies for desalination, Desalination, 245 (2009) 214–231.
[48] H. Chang, S.-G. Lyu, C.-M. Tsai, Y.-H. Chen, T.-W. Cheng, Y.-H. Chou, Experimental and simulation study of a solar thermal driven membrane distillation desalination process, Desalination, 286 (2012) 400–411.
[49] E. Guillén-Burrieza, G. Zaragoza, S. Miralles-Cuevas, J. Blanco, Experimental evaluation of two pilot-scale membrane distillation modules used for solar desalination, J. Membr. Sci., 409 (2012) 264–275.
[50] A.P. Straub, N.Y. Yip, S. Lin, J. Lee, M. Elimelech, Harvesting low-grade heat energy using thermo-osmotic vapour transport through nanoporous membranes, Nat. Energy, 1 (2016) 1–6.
[51] A. Kullab, A. Martin, Membrane distillation and applications for water purification in thermal cogeneration plants, Sep. Purif. Technol., 76 (2011) 231–237.
[52] V.A. Bui, L.T. Vu, M.H. Nguyen, Simulation and optimisation of direct contact membrane distillation for energy efficiency, Desalination, 259 (2010) 29–37.
[53] F. He, J. Gilron, H. Lee, L. Song, K.K. Sirkar, Potential for scaling by sparingly soluble salts in crossflow DCMD, J. Membr. Sci., 311 (2008) 68–80.
[54] M. Khayet, C. Cojocaru, C. García-Payo, Application of response surface methodology and experimental design in direct contact membrane distillation, Ind. Eng. Chem. Res., 46 (2007) 5673–5685.
[55] F. Macedonio, E. Drioli, Pressure-driven membrane operations and membrane distillation technology integration for water purification, Desalination, 223 (2008) 396–409.
[56] M. De Andres, J. Doria, M. Khayet, L. Pena, J. Mengual, Coupling of a membrane distillation module to a multieffect distiller for pure water production, Desalination, 115 (1998) 71–81.
[57] A.N.A. Mabrouk, Y. Elhenawy, G. Mostafa, M. Shatat, M. El-Ghandour, Experimental Evaluation of Novel Hybrid Multi Effect Distillation–Membrane Distillation (MED-MD) Driven by Solar Energy, Desalination for the Environment: Clean Water and Energy Rome, Rome, Italy, 2016, pp. 22–26.
[58] A.E. Khalifa, S.M. Alawad, M.A. Antar, Parallel and series multistage air gap membrane distillation, Desalination, 417 (2017) 69–76.
[59] A. Omar, A. Nashed, Q. Li, R.A. Taylor, Experimental and numerical evaluation of the energy requirement of multi-stage vacuum membrane distillation designs, Sep. Purif. Technol., 257 (2021) 117303, doi: 10.1016/j.seppur.2020.117303.
[60] A.V. Dudchenko, T.V. Bartholomew, M.S. Mauter, Cost optimization of multi-stage gap membrane distillation, J. Membr. Sci., 627 (2021) 119228, doi: 10.1016/j.memsci.2021.119228.
[61] N. Dutta, B. Singh, S. Subbiah, P. Muthukumar, Performance analysis of a single and multi-staged direct contact membrane distillation module integrated with heat recovery units, Chem. Eng. J. Adv., 4 (2020) 100055, doi: 10.1016/j.ceja.2020.100055.
[62] A.K. Fard, Y.M. Manawi, T. Rhadfi, K.A. Mahmoud, M. Khraisheh, F. Benyahia, Synoptic analysis of direct contact membrane distillation performance in Qatar: a case study, Desalination, 360 (2015) 97–107.
[63] E. Ali, J. Orfi, An experimentally calibrated model for heat and mass transfer in full-scale direct contact membrane distillation, Desal. Water Treat., 116 (2018) 1–18.
[64] A. Najib, J. Orfi, E. Ali, A. Ajbar, M. Boumaaza, K. Alhumaizi, Performance analysis of cascaded membrane distillation arrangements for desalination of brackish water, Desal. Water Treat., 76 (2017) 19–29.
[65] O. Jamel, N. Abdullah, A. Emad, A. Abdulhamid, A. Maher, B. Mourad, A. Khalid, Membrane distillation and reverse osmosis based desalination driven by geothermal energy sources, Desal. Water Treat., 76 (2017) 40–52.
[66] J. Gilron, L. Song, K.K. Sirkar, Design for cascade of crossflow direct contact membrane distillation, Ind. Eng. Chem. Res., 46 (2007) 2324–2334.
[67] J.O.E. Ali, A. Najib, Thermodynamic analysis of direct contact membrane distillation with/without heat recovery based on experimental data, Desal. Water Treat., 466 (2019) 52–67.
[68] E.A.A. Najib, K. Al-Humaizi, A. Ajbar, J. Orfi, M. Boumaza, Performance analysis of cascaded membrane distillation arrangement of desalination of brackish water, Desal. Water Treat., 76 (2017) 19–29.
[69] A.N.J. Orfi, E. Ali, A. Ajbar, M. AlMatrafi, M. Boumaaza, K. Albumenize, Membrane distillation and reverse osmosis-based desalination driven by geothermal energy sources, Desal. Water Treat., 76 (2017) 40–52.
[70] M. Khayet, Desalination by Membrane Distillation, Encyclopedia of Life Support Science (EOLSS), Water and Wastewater Treatment Technologies, 2010.
[71] K. Nakoa, A. Date, A. Akbarzadeh, A research on water desalination using membrane distillation, Desal. Water Treat., 56 (2015) 2618–2630.

[72] D. González, J. Amigo, F. Suárez, Membrane distillation: perspectives for sustainable and improved desalination, Renewable Sustainable Energy Rev., 80 (2017) 238–259.
[73] Y.M.M.K. Fard, Y. Rhadfi, K.A. Mahmoud, M. Khraisheh, F. Benyahia, Synoptic analysis of direct contact membrane distillation performance in Qatar: a case study, Desalination, 360 (2015) 97–107.
[74] D. Winter, J. Koschikowski, M. Wieghaus, Desalination using membrane distillation: Experimental studies on full scale spiral wound modules, J. Membr. Sci., 375 (2011) 104–112.

Appendix A

The purification of water by direct contact membrane distillation is managed by the coupled mass and heat-transfer mechanisms. The model of the membrane distillation process governing the mass and heat transfer operation is widely published and used [63,67–69]. Hence a short description of the model will be listed here. Assuming steady state conditions:

The mass flux can be computed by the following equation:

$$j_w = C_m\left(P_1 - P_2\right) \tag{A1}$$

The vapor pressure, at the membrane interface, is calculated by the following [70]:

$$P_1 = \exp\left(23.238 - \frac{3841}{T_{\text{hm}} - 45}\right)\left(1 - C_s\right)\left(1 - 0.5C_s - 10C_s^2\right) \tag{A2}$$

$$P_2 = \exp\left(23.238 - \frac{3841}{T_{\text{cm}} - 45}\right) \tag{A3}$$

where T_{h_m} and T_{c_m} are the hot and cold temperatures at the membrane interface.

The membrane coefficient, C_m, can be computed based on the active mechanism by the membrane properties and the average membrane temperature, that is, $T = \frac{T_{h_m} + T_{c_m}}{2}$. The active mechanism was determined under the following conditions [71]:

- the Knudsen flow mechanism, $k_n > 1$:

$$C_m^k = \frac{2\varepsilon r}{3\tau\delta}\left(\frac{8M_w}{\pi RT}\right)^{1/2} \tag{A4}$$

- Molecular diffusion mechanism, $k_n < 0.01$:

$$C_m^D = \frac{\varepsilon}{\tau\delta}\frac{PD}{P_a}\frac{M_w}{RT} \tag{A5}$$

- Knudsen–molecular diffusion transition mechanism, $0.01 < k_n < 1$:

$$C_m^C = \left[\frac{3}{2}\frac{\tau\delta}{\varepsilon r}\left(\frac{\pi RT}{8M_w}\right)^{1/2} + \frac{\tau\delta}{\varepsilon}\frac{P_a}{PD}\frac{RT}{M_w}\right]^{-1} \tag{A6}$$

where the Knudsen number, defined as $k_n = \lambda/d$, and where λ is the mean free path of water molecules, further expressed as Eq. (A7) [72]:

$$\lambda = \frac{k_B T}{\sqrt{2}\pi P d_e^2} \tag{A7}$$

where T and P are the average temperature and pressure, at the membrane interface, respectively, $k_B = 1.380622 \times 10^{-23}$ and $d_e = 9.29 \times 10^{-20}$.

The membrane interface temperatures (T_{h_m}, T_{c_m}) can be found by solving the combined mass and energy balance. At a steady state, the different heat-transfer mechanisms become equal. These equalities translate into the following expressions [71]:

$$U\left(T_{h_b} - T_{c_b}\right) = h_f\left(T_{h_b} - T_{h_m}\right) = j_w h_v + h_m\left(T_{h_m} - T_{c_m}\right) \tag{A8}$$

$$U\left(T_{h_b} - T_{c_b}\right) = h_p\left(T_{c_m} - T_{c_b}\right) = j_w h_v + h_m\left(T_{h_m} - T_{c_m}\right) \tag{A9}$$

The above equalities can be solved iteratively to calculate the values of T_{h_m} and T_{c_m} employing the existing bulk temperatures ($T_{h_b} = T_{h_{\text{in}}}, T_{c_b} = T_{c_{\text{in}}}$) for the hot and cold channels, the heat-transfer coefficients of the film (h_f, h_p) could be estimated by the Nusselt number, as follows [72]:

$$\text{Nu} = 0.298\,\text{Re}^{0.646}\,\text{Pr}^{0.316} \tag{A10}$$

where Re is the Reynolds number and Pr is the Prandtl number.

The latent heat of vaporization, at the average membrane temperature, is calculated by the following equation [73]:

$$h_v\left(T\right) = 1850.7 + 2.8273\text{T} - 1.6 \times 10^{-3}T^2 \tag{A11}$$

The overall heat-transfer coefficient was calculated, as follows [71]:

$$U = \left[\frac{1}{h_f} + \frac{1}{h_m + \dfrac{J_w h_v}{T_{h_m} - T_{c_m}}} + \frac{1}{h_p}\right]^{-1} \tag{A12}$$

where h_m is the heat-transfer coefficient of the membrane, which involves the conduction resistance. It is computed, as follows [74]:

$$h_m = \frac{k_m}{\delta} = \frac{\left(1 - \varepsilon\right)k_s + \varepsilon k_g}{\delta} \tag{A13}$$